

See discussions, stats, and author profiles for this publication at: <https://www.researchgate.net/publication/263949922>

Efficiency Enhancement in ZnO:Al-Based Dye-Sensitized Solar Cells Structured with Sputtered TiO₂ Blocking Layers

ARTICLE *in* THE JOURNAL OF PHYSICAL CHEMISTRY C · MARCH 2014

Impact Factor: 4.77 · DOI: 10.1021/jp411811q

CITATIONS

10

READS

57

7 AUTHORS, INCLUDING:



Alessandra Alberti

Italian National Research Council

83 PUBLICATIONS 427 CITATIONS

[SEE PROFILE](#)



Guglielmo Condorelli

University of Catania

127 PUBLICATIONS 1,945 CITATIONS

[SEE PROFILE](#)



Antonino La Magna

Italian National Research Council

263 PUBLICATIONS 1,850 CITATIONS

[SEE PROFILE](#)



Tsutomu Miyasaka

ToIn University of Yokohama

115 PUBLICATIONS 6,365 CITATIONS

[SEE PROFILE](#)

Efficiency Enhancement in ZnO:Al-Based Dye-Sensitized Solar Cells Structured with Sputtered TiO₂ Blocking Layers

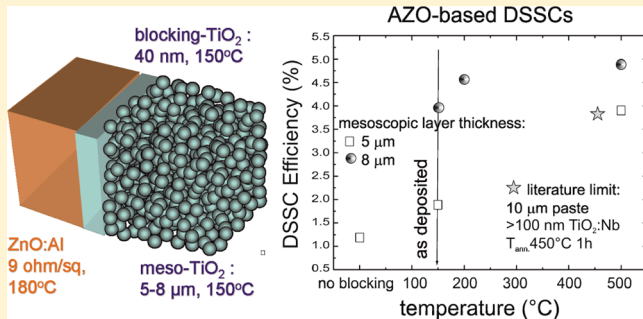
A. Alberti,^{*,†} G. Pellegrino,[†] G. G. Condorelli,[‡] C. Bongiorno, S. Morita,[§] A. La Magna, and T. Miyasaka[§]

[†]CNR-IMM Zona industriale, Strada VIII 5, 95121, Catania, Italy

[‡]Università degli Studi di Catania and INSTM UdR Catania, Viale Andrea Doria 6, Catania, Italy

[§]Graduate School of Engineering, Toin University of Yokohama, 1614 Kuroganecho, Aoba, Yokohama 225-8503, Japan

ABSTRACT: We explored new strategies for efficiency enhancement in dye-sensitized solar cells (DSSCs) by combining dehydration–condensation reactions with sputtering deposition methods. The photoanodes were realized by means of low-temperature preparation of mesoporous TiO₂ films on thin undoped TiO₂ compact (blocking) layers on ZnO:Al (AZO) substrates and sensitization with ruthenium dye, N719. For photoanodes fabrication, an 8 μm thick mesoporous film of TiO₂ and an under critical thermal budget, applied before dye loading (≤ 200 °C; i.e., 150 °C for the TiO₂ mesoscopic layer and 200 °C for the TiO₂ blocking/AZO bilayer), were employed, which renders the overall process competitive for the applications. The structural properties of the sputtered TiO₂/AZO bilayer were optimized, and a cell efficiency as high as the 4.6%, above the current literature limit for AZO-based DSSC (3.8% for 10 μm thick mesoporous layers sintered at 450 °C and sensitized with N719), was achieved at $T \leq 200$ °C. With the proposed scheme for the photoanode structure and using, instead, a conventional thermal treatment at 500 °C (30 s), the cell efficiencies were further raised up to 4.9%. It was thus evidenced that the use of optimized materials for the cell architecture makes the AZO-based DSSC nowadays rising devices.



1. INTRODUCTION

Dye-sensitized solar cells (DSSC) are attracting the scientific community due to the large versatility and the low production cost.¹ They are especially attractive for integrated building photovoltaic applications for which a less severe effect of the photon incident angle on the light harvesting efficiency is expected.² Overall light-to-electric energy conversion efficiency of 7% in simulated solar light has been recently improved up to 13%.³ All the high efficiency values reported in the literature were achieved by using sintering processes in the range of 450–500 °C, therefore useful for glass technologies but not compatible with flexible substrates. It is well-known that the quantum efficiency of the device depends on the light harvesting efficiency (LHE), the quantum yield for electron injection (ϕ_{inj}), and the electron collection efficiency (η_{coll}) by the transparent conductive oxide (TCO). F-doped SnO₂ (FTO) is a single TCO which allows high-temperature sintering process. However, electrical conductivity of FTO is relatively low, and it is more difficult to pattern via wet etching as compared to ITO.⁴ Indium tin oxide (ITO) has also been used as TCO of DSSCs in condition of low-temperature processes. Despite the good electrical conductance, ITO lacks in current rectification ability as semiconductor due to high carrier density ($10^{19–20}/cm^3$). The use of indium is also an issue for the environment compatibility. Among the TCOs, Al-doped Zn oxides (AZO) are recently becoming attractive candidates

thanks to the abundance and nontoxicity of the elements and to the versatility of the doping procedure (also at low temperature).⁴ AZO layers can offer low resistivity (<mΩ·cm), high mobility values, and high transparency in the visible wavelength range (up to 90% transmittance or even higher). AZO also shows better chemical stability to hydrogen plasmas, better thermal stability, and lower cost with respect to the commonly used ITO.⁴ The use of vacuum equipment to realize conductive AZO layers offers huge advantages in terms of reproducibility of the process and realization of multiple anodes on large areas in a single-run process. This would guarantee a very high production throughput which is mandatory to reduce the cost of the cell, also nowadays sensibly affected by the cost of tin-based TCOs.

One of the approaches to apply AZO as TCO of DSSC is by coating the surface of AZO with a TiO₂ nonporous compact layer and by subsequently superimposing to that bilayer a TiO₂ mesoporous layer prepared with a nanopastes of titania. The array of TiO₂ nanoparticles serves as “bulk” material for the sensitization process since it offers a high surface to volume ratio needed to improve the dye loading as well as the light-absorbing power in the device. The conventional method of

Received: December 2, 2013

Revised: March 5, 2014

Published: March 10, 2014

preparing mesoporous TiO_2 materials requires the high-temperature sintering of a binder-containing viscous TiO_2 nanopastes on TCO substrate. Sintering of the nanopastes is the prerequisite to eliminate the insulating polymer binders from the TiO_2 layer. This sintering process however causes contamination of impurities (residual carbon, etc.) that can lower the conduction band level and photovoltage of the TiO_2 electrode. In a different approach, highly crystalline and purified TiO_2 can be realized by low temperature, sinter-free preparation of the TiO_2 layer, which is based on chemical synthesis of mesoporous TiO_2 by the dehydration-condensation reaction.^{5,6} Sinter-free low-temperature TiO_2 coating is one of promising printable technologies which can minimize the device assembling time and realize a significant cost reduction in cell manufacture.^{7,8}

On the other hand, the use of a TiO_2 blocking between the AZO and the mesoporous layer represents a promising choice to improve the cell performances and efficiency.^{9–13} The TiO_2 compact layer serves to several purposes: to protect the AZO surface against corrosion by the electrolytic solution (protective layer), to improve the electrical coupling between the mesoscopic layers and the AZO surface (coupling layer), and to reduce the back-recombination process of the injected carriers (blocking layer). Therefore, for the role played by that layer in the device architecture, its interfacial properties must be carefully investigated and optimized,^{14–18} and in particular, the thermal budget and the thickness to achieve adequate coupling/blocking layers need to be further reduced. An appropriate control and a large reproducibility of the processes over large area are offered by the sputtering depositions.¹⁹ Operating in the oxidized mode, an appropriate tuning of the layer stoichiometry and transparency can be done. The main limitation by operating in the oxidized mode is that the TiO_2 layer has usually an amorphous structure at room temperature, unless a postdeposition thermal treatment at $T \geq 300$ °C²⁰ is added or if high power loadings for long deposition times are applied.^{21,22}

The AZO substrate serves as collector of the photoelectrons injected through the dye/ TiO_2 interface. In this respect, it is well-known that the AZO structure (e.g., texturing, Al content) and the surface exposed to the TiO_2 deposition^{17,18,23} are crucial to tailor the behavior of the cell. AZO-based DSSCs have, up to now, efficiencies in the range between 1.9 and 3.8% with use of N719 dye, with a gain recently achieved by using a niobium-doped TiO_2 blocking layer (e.g., 100 nm) over AZO²⁴ or over AZO/Ag/AZO multilayer structures.²⁵ The $\text{TiO}_2\text{:Nb}$ layer was found to block oxygen diffusion into AZO during air-annealing and to suppress the formation of Zn^{2+} -dye aggregates at the AZO surface. In all those cases, a thermal budget in the range of 450–500 °C is needed for the TiO_2 nanopastes sintering process.

In this work we propose an AZO-based approach to realize competitive DSSCs employing an undoped and continuous ~40 nm thick TiO_2 blocking layer and a mesoporous array of low-temperature (LT)-prepared nano- TiO_2 grains. For that purpose, the TiO_2 mesoporous array was made by sinter-free dehydration-condensation reactions, while the TiO_2 compact layers was realized by dc reactive sputtering deposition on thick sputtered AZO substrates. We show that, with an appropriate tuning of the structural properties of the TiO_2 blocking/AZO bilayer, in combination with the use of a proper sinter-free TiO_2 nanopastes, the efficiency of the DSSC can significantly overcome the current literature limit even by using low-

temperature methods of preparation ($T \leq 200$ °C). Such high performances were comparable to or even better than those achieved in the literature for DSSCs prepared through low-temperature processes on ITO or FTO (e.g., 4% with 10 μm thick mesoporous TiO_2 on ITO;²⁶ 2.47% with 4 μm thick mesoporous TiO_2 on FTO as TCO;²⁷ 4.3% with the mesoporous TiO_2 on ITO/PEN treated by UV irradiation²⁸).

Our findings thus open a scenario such that (1) just in a double-step process, (2) in the same sputtering equipment, (3) over large areas, (4) with large reproducibility and uniformity, and (5) by using a low cost TCO a DSSC industry can aim at a large production throughput with a high quality control of the TiO_2 -blocking/AZO bilayer.

2. EXPERIMENTAL SECTION

ZnO:Al (AZO) layers were deposited on corning glass substrates (1737) by dc-pulsed sputter deposition using a Symmorphix 1600 equipment from a composite ZnO:Al rectangular target (98 wt % ZnO and 2 wt % (Al_2O_3), 64 × 55 cm^2) with an Ar flow rate of ~20 sccm and a sputtering power of ~350 W, at an effective temperature of 180 °C (as measured by a thermostrips placed on top of the sample). By using these process parameters, a deposition rate of 0.15 nm/s was achieved and used to deposit ~900 nm thick AZO layers. The electrical conductivity was evaluated by sheet resistance analyses which give an average value as low as 9.2 ohm/square, which corresponds to a resistivity of ~1 $\text{m}\Omega\cdot\text{cm}$.

A compact layer composed of TiO_x (x to be determined, see the experimental part) was deposited on AZO by using a dc reactive sputtering equipment (Kenotec) starting from a pure titanium target. The process was carried out by applying a constant power of ~600 W (1.24 A, 498 V, power loading 4.9 W/cm^2) for 480 s and by setting the external heater in such a way that the value measured on the sample surface was ~150 °C. The temperature on the sample surface was measured by using commercially available thermostrips taped on the AZO surface. An O_2/Ar flow rate ratio as low as of 5/45 sccm was set in order to maintain a low growth rate (3.7 nm/min) and to guarantee the proper layer stoichiometry. The process was set in the oxidized mode (in the low deposition rate regime) at a pressure of 0.85 Pa with an anode–cathode distance of 10 cm, which implies (by also considering the power loading, the deposition time, and the sputtering current values used) a moderate temperature rise due to the plasma contribution itself if compared to the increase due to the external heating. Each deposition process is preceded by a presputtering step to clean up the surface of the Ti target and to remove residual thin oxide layer. This sputtered TiO_2 layer will be called blocking layer. The TiO_2 blocking/AZO bilayer was annealed ex situ in dry air ($\text{N}_2:\text{O}_2 = 78\%:22\%$) at 200 °C for 30 min or at 500 °C for 30 s, using a Jipelec Jetfirst 150 system equipped with a tubular infrared heating lamps and a thermocouple for an accurate control in the low temperature regime.

To realize the devices, the TiO_2 blocking layer was selectively sputtered on AZO over an active area of 0.5 cm × 0.5 cm and subsequently coated with a mesoporous array of TiO_2 nanoparticles, preliminary cleaned by UV-ozone treatments, by the doctor-blade coating method. A binder-free type mesoscopic TiO_2 nanopastes^{5,6} is used for this coating which is specially prepared for low-temperature film deposition. The coated wet layer was dried at room temperature for 30 min and treated by subsequent heating under air at 150 °C for 10 min. For photoelectrode preparation, the TiO_2 -coated AZO

electrode was dipped in a 0.3 mM solution of Ru complex dye, N719, in a mixture of *tert*-butanol:acetonitrile:ethanol (2:1:1) at 40 °C for 2 h for dye adsorption and sensitization of the mesoscopic TiO₂ surface. Here, two different thicknesses of the mesoscopic layers, 5 and 8 μm, were used to modulate the dye loading amount. DSSC was assembled by combining the photoelectrode (anode) with a Pt-sputtered FTO glass counter electrode (cathode), which gave an active area of irradiation, 0.24 cm². The electrolyte used in DSSC comprised 0.02 M I₂, 0.4 M LiI, 0.4 M tetrabutylammonium iodide, and 0.3 M 1-methylbenzimidazole in acetonitrile. By combining differently annealed TiO₂ blocking layers with nano-TiO₂ pastes having different thickness, we intend to optimize the cell performances on AZO.

Several analytical techniques were used to investigate and correlate the structure of the photoanode components (TiO₂mesoscopic layers/TiO₂blocking/AZO/glass) to the electrical behavior of the cells. The structural characterization of the deposited multilayers materials was performed by X-ray diffraction (XRD) and X-ray reflectivity (XRR) by using a D8-Discover Bruker AXS diffractometer, equipped with a Cu K α source. Transmission electron microscopy (TEM) and electron diffraction analyses were done using a JEOL JEM 2010 microscope operating at 200 kV. UV-vis measurements were carried out on a UV-vis V-650 JASCO spectrophotometer, and the spectra were recorded with a ±0.2 nm resolution. Film surface morphology was examined by field emission scanning electron microscopy (FESEM) using a ZEISS VP 55 microscope. The atomic composition of the films was analyzed by energy dispersive X-ray analysis (EDX), using an INCA-Oxford windowless detector. Thickness measurement and surface morphology investigation for blocking TiO₂ and mesoporous TiO₂ film were done with a Veeco DEKTAK 150 profilometer in combination with a Keyence digital microscope.

For the measurement of the device performances, a solar simulator as the light source (PEC L10, Peccell Technologies) and an incident-photon-to-current conversion efficiency (IPCE) system (PEC S20, Peccell Technologies) were used to monitor the photocurrent–voltage (*J*–*V*) and the conversion efficiency of the device under illumination. Light intensity from the solar simulator was adjusted as AM1.5 100 mW/cm² (1 sun) by means of a standard silicon photocell. Electrochemical impedance spectroscopy (EIS) for Nyquist plots was conducted by means of a Princeton VSP/Z-01 potentiostat with ac amplitude of 10 mV in a frequency range from 200 kHz to 1 Hz at an open circuit (*V*_{oc}) condition under 1 sun illumination.

3. RESULTS AND DISCUSSION

3.1. DSSC Characterization. In Figure 1a, we show the photocurrent density–voltage (*J*–*V*) curves related to AZO-based cells (5 μm mesoporous array of TiO₂) having the TiO₂-blocking/AZO bilayer left as deposited or annealed at 500 °C, in comparison with the case of a cell without the blocking layer. The thermal treatment was done before mesoscopic layer deposition and dye loading. From the comparison it emerges that the use of a thin (~40 nm) blocking layer, without any doping procedure, allows improving all the cells parameters, i.e., the short circuit current (*J*_{sc}), the open circuit voltage (*V*_{oc}), and also the cell efficiency with respect to the reference values. All the values are given in Table 1. The best performances were achieved by using a blocking layer preannealed at 500 °C. In Figure 1b, the order of IPCE values, cell 3 > cell 1 > cell ref, are

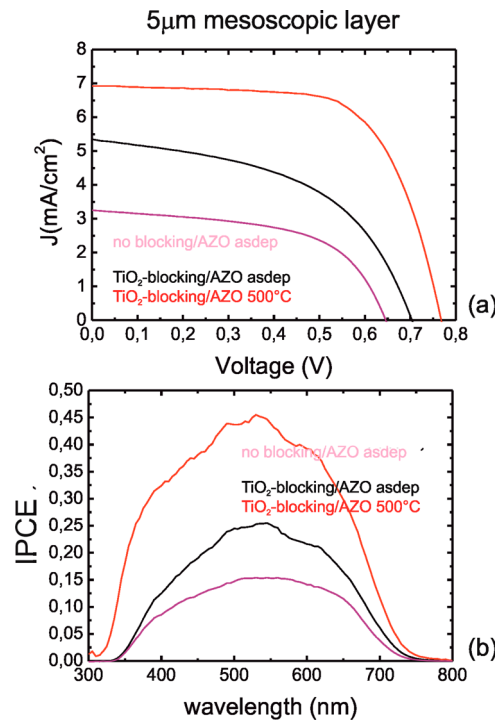


Figure 1. *J*–*V* (a) and IPCE (b) of AZO-based DSSCs which employ TiO₂-blocking layers on AZO. The annealing at 500 °C, 30 s, was done before mesoscopic layers deposition and dye loading. The thickness of the low-temperature (LT)-prepared mesoporous TiO₂ films is 5 μm. The reference cell, without the TiO₂ blocking layer, is also shown for comparison.

Table 1. Cell Parameters as a Function of the Preparation Procedure for the TiO₂-Blocking/AZO Bilayer^a

conditions	cell no.	<i>J</i> _{sc} (mA cm ⁻²)	<i>V</i> _{oc} (V)	fill factor	efficiency (%)
no blocking-TiO ₂ + LT TiO ₂	ref	3.25	0.65	0.56	1.19 ± 0.05
blocking-TiO ₂ as deposited + LT TiO ₂	1	5.35	0.70	0.50	1.89 ± 0.07
blocking-TiO ₂ 500 °C (30 s)+ LT TiO ₂	3	7.65	0.75	0.68	3.90 ± 0.15

^aThe thickness of the mesoscopic layers is 5 μm.

in good agreement with the variation of photocurrent densities (*J*) between the cells.

The cell performances were further improved by changing the thickness of the TiO₂ mesoporous array. The data are shown in Figure 2 as a function of the annealing temperature performed on the TiO₂-blocking/AZO bilayer before mesoscopic layers deposition. The mesoscopic layers were treated at a temperature of 150 °C in all cases, before the sensitization process.

From the comparison (Figure 2d) it can be observed that by applying a thermal budget on the TiO₂-blocking/AZO bilayer (before mesoscopic TiO₂ deposition) instead of using sintering processes (500 °C) over the entire structure (including the mesoporous array), we obtained the highest efficiency for AZO-based DSSC among those reported which use 10 μm thick mesoporous TiO₂ sensitized with N719,²² even by reducing the TiO₂ thickness to 5 μm. Furthermore, by increasing the mesoporous TiO₂ layer thickness to 8 μm (<10 μm²⁴), the efficiency of the cells overcomes the literature limit, assessing to

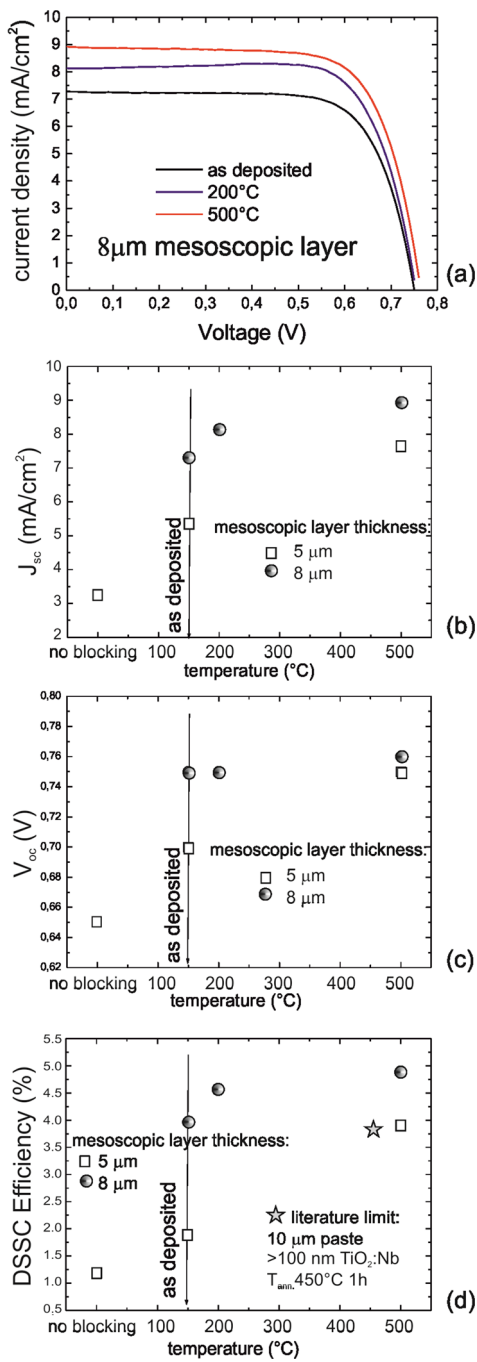


Figure 2. (a) J - V curves, (b) J_{sc} , (c) V_{oc} , and (d) efficiency modulation by changing the mesoporous TiO₂ thickness. The data are plotted as a function of the temperature used to anneal the TiO₂-blocking/AZO bilayer before mesoscopic layer deposition. The arrows indicate the cells with the TiO₂-blocking/AZO bilayer left as deposited (TiO₂ deposition temperature = 150 °C). The annealing times were 30 min at 200 °C and 30 s at 500 °C. In (d) a reference value was also reported (the star) which refers to a cell having, with respect to our data, a thicker and doped TiO₂ blocking layer and also a thicker mesoporous array of TiO₂. In all cases, the cells were sensitized with N719.

a value as high as the 4.9%. The cell efficiency values can be related to the combined effects of the short-circuit current density (J_{sc}), the open circuit voltage (V_{oc}), and the fill factor (FF) by the formula $\eta = V_{oc} \times J_{sc} \times FF / P_{in}$. Increasing the mesoscopic layer thickness from 5 to 8 μm produces a

systematic increase of the J_{sc} values (Figure 2a), with, on the other hand, a less pronounced gain in the V_{oc} values (Figure 2b). In that range, also the fill factor systematically increases from 68% to 72% by increasing the mesoscopic layers thickness (from 5 to 8 μm). It is further noteworthy that the efficiency of the cells can be maintained competitively high even by reducing the thermal treatment on the TiO₂-blocking/AZO to 200 °C, thus allowing keeping the overall thermal budget on the cell at $T \leq 200$ °C (i.e., 150 °C for the mesoscopic layer, 200 °C for the blocking layer/AZO). Also, the scheme without any additional thermal treatment (see arrow in Figure 2c) can become of interest ($T < 200$ °C: i.e., 150 °C for the nano-TiO₂ pastes, 150 °C for the blocking layer, 180 °C for the AZO).

It can be thus summarized that (1) the blocking layer, although it is thin and undoped, has a severe effect on the cell performances, (2) a cell efficiency above the current literature limit is accessible even by reducing the thickness of the TiO₂ mesoscopic layer or drastically reducing the thermal budget on the photoanode (before dye sensitization), and (3) the cell efficiency can get a value as high as the 4.9% by an appropriate tuning of the TiO₂-blocking/AZO bilayer. It was additionally observed by J - V analyses in dark conditions that the cells having the TiO₂-blocking/AZO bilayer left as deposited or annealed at 200 °C have lower parasitic diode currents than the others, with the worst case offered by the cell without blocking layer (from 3 to 12 mA/cm²). This implies that the blocking layer is actually efficacious to block the backward current from the parasitic diode.

3.2. Mesoscopic Layer Composition by XRD. The mesoscopic layer composition was investigated by X-ray diffraction in symmetric and also in grazing incidence configurations. By using the symmetric geometry, such that the incident angle is equal to the exit angle, texturing along preferential growth axes was not observed (symmetric XRD). In all cases, the phase formed is TiO₂, mainly in the anatase (hereafter called A) and rutile (hereafter called R) polymorphisms. The average domain size of the nano-TiO₂ domains, following the Debye–Scherrer equation, is 18 ± 1 and 29 ± 3 nm for A and R, respectively. Those findings are independent of the blocking layer used. The grazing geometry, with an incident angle of 0.4°, allowed largely confining the beam into the mesoscopic layer to a depth of ~100 nm. The results are shown in Figure 3a as a function of the temperature used for the pretreatment of the TiO₂-blocking/AZO substrates. In the diffraction pattern, a unique AZO peak is present (at $2\theta = 62.8^\circ$, (10–13) planes), and this is in agreement with the preferential texturing of the AZO layer along the [0001] growth axis. Its presence derives by the fact that the size of the X-ray beam used is, on one side, larger than the size of the photoanode active area (5 mm × 5 mm, see experimental part). In the figure, the colored bars indicate the random references for the different TiO₂ polymorphisms. Anatase was found to be dominant, with a certain amount of rutile and a very little amount of brookite in the mixture. To quantify the percentage of anatase with respect to the R + A amount (the brookite part is negligible), we used a well-known approach reported in the literature by Spurr–Myers:^{29,30} as usual, the semiempirical equation was applied to the (101) anatase and to the (110) rutile peaks. The main hypothesis of the model, about the absence of texturing in the mixed system, was preliminarily verified by the symmetric XRD scans. With this approach a percentage of anatase above the 94% was found in all the samples (Figure 3b).

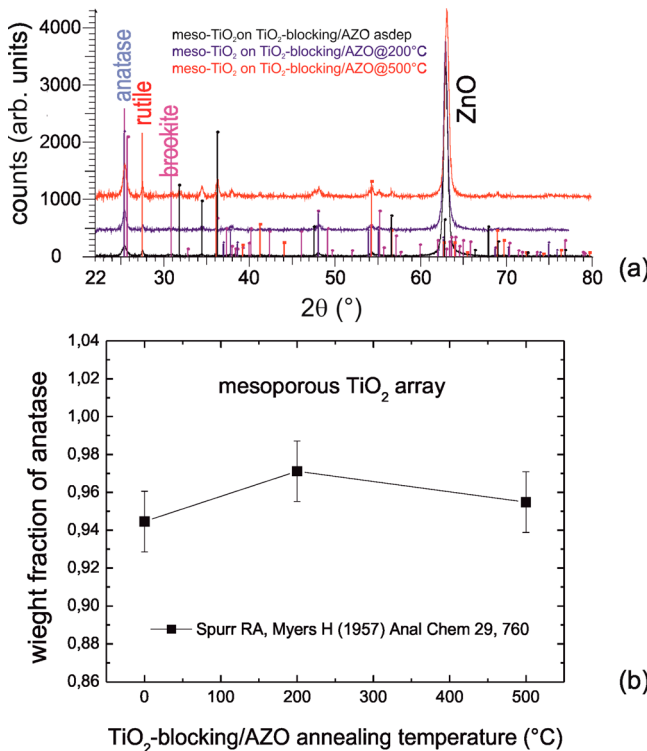


Figure 3. (a) Diffraction patterns of the TiO₂ mesoscopic layer, collected in grazing incidence (0.4°) configuration, as a function of the temperature of the pretreatment of the blocking/AZO substrate in dry air at different temperatures. (b) Weight fraction of the anatase polymorphism vs the A + R amount in the mesoscopic layer array. All the deposited mesoscopic layers have a predominance of the anatase, with a percentage of ~96% (comparable in all cases, within the error bars).

3.3. Morphology of the Mesoscopic Layer and of the Blocking Layer Underneath. The morphology of the TiO₂ mesoscopic layer was evaluated by SEM analyses, as shown in Figure 4a: it is porous with wide canyons largely protruding into the layer. The surface of the TiO₂ blocking layer was also investigated, before mesoscopic layer deposition, as shown in Figure 4b: the surface is quite rough but without canyons. The roughness derives from the AZO substrate morphology, since the TiO₂ blocking layer makes a conformal coverage on AZO, as will be discussed in what follows.

After having characterized the mesoscopic layer and since it does not differ from sample to sample, we now focus on the

structural characterization of the blocking-TiO₂/AZO bilayers, before and after annealing, with the intent of correlating the structural data to the electrical results. The TEM cross section of the TiO₂-blocking/AZO bilayer structure, left as deposited, is shown in Figure 5a. The TiO₂-blocking layer creates a

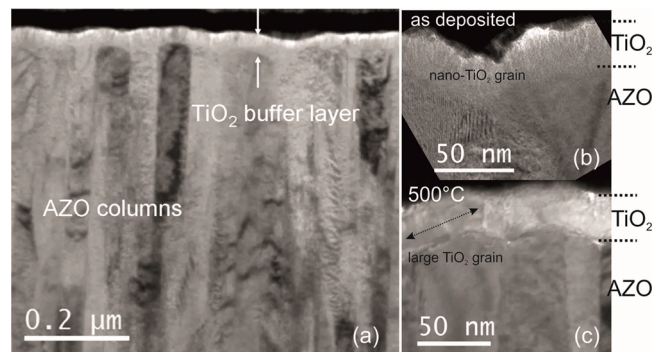


Figure 5. (a, b) Cross-sectional TEM analyses of the as deposited TiO₂-blocking/AZO bilayer structure. The AZO grains have a columnar structure, with a rough surface. The blocking layer is conformal and continuous over that surface, also after annealing (c), but with larger grains.

conformal coverage over the AZO substrate, with a uniform thickness of ~40 nm. The AZO layer is characterized by columnar grains extending for most of the layer thickness. Those grains are fiber textured mainly following the [0001] growth axis,¹⁵ as already discussed about the analysis in Figure 3a. The conformity of the coverage and the layer thickness do not significantly change after annealing at 200 °C or at 500 °C. In the selected area of Figure 5b it can be observed that the blocking layer protects the AZO surface by creating a compact and continuous layer in the immediate proximity of the AZO surface, and this effect is independent of the thermal treatment. As a difference between the as-deposited (similar to the 200 °C annealed layer) and the 500 °C annealed layer, the TiO₂ layer gains a further compactness in its uppermost part after annealing at 500 °C. Additionally to that, the 500 °C annealing process produces a severe increase of the TiO₂ domain size (Figure 5c).

Figure 6 shows the plan-view TEM analyses of the TiO₂-blocking layer over the AZO substrate before (a) and after (b) annealing at 500 °C (30 s) in dry air. The TiO₂-blocking layer, after deposition at 150 °C and also after postdeposition annealing at 200 °C, has a porous structure, with relatively

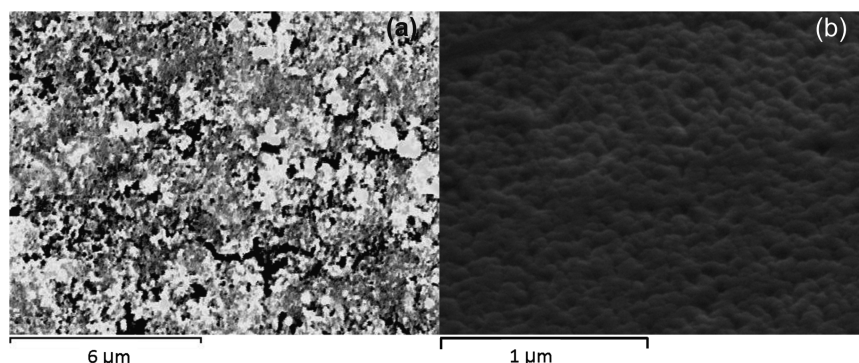


Figure 4. (a) As-deposited TiO₂ mesoporous film morphology over the blocking layer. (b) As-deposited TiO₂ blocking layer morphology. The TiO₂ layer (5 μm) is porous, with large canyons.

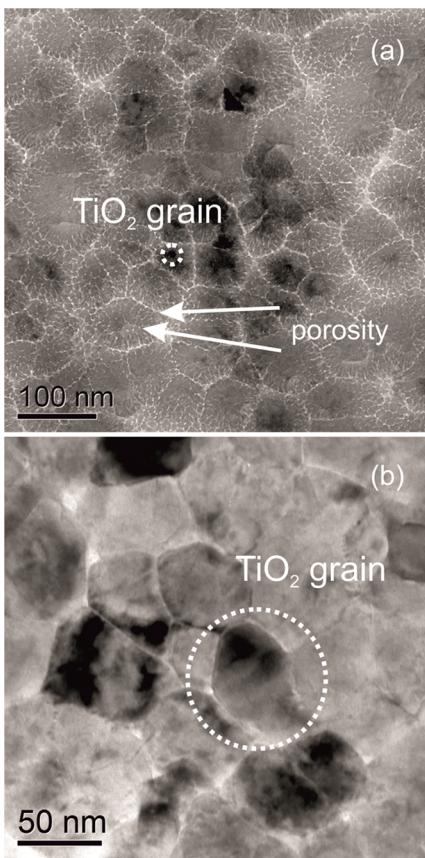


Figure 6. Plan view TEM analyses of the TiO_2 -blocking layer over the AZO substrate: (a) as deposited; (b) after annealing at $500\text{ }^\circ\text{C}$. The grain size and porosity of the TiO_2 -blocking layer are affected by the annealing process.

small TiO_2 domains (in the range of 8–30 nm, see Figure 8b) seated over the large AZO grains (100–200 nm in diameter). This porosity arises from the uppermost part of the layer, while the portion of the layer in contact with the AZO surface is more compact. The intergrain porosity is largely reduced after postdeposition annealing at $500\text{ }^\circ\text{C}$, as the TiO_2 domain size increases up to values of ~ 40 –80 nm (Figure 6b). The reduction of the layer porosity is expected to have a role in the structural/electrical coupling between the blocking layer and the mesoporous array and consequently on the carrier injection toward the blocking- TiO_2 /AZO substrate.

3.4. TiO_2 -Blocking Layer Composition and Average Microstructure by XRD. Since the thermal treatments over the TiO_2 -blocking/AZO bilayer, performed before TiO_2 mesoscopic layer deposition, trigger severe structural modification in the TiO_2 -blocking layer, we closely investigated the blocking layer structure modification in the range between 200 and $500\text{ }^\circ\text{C}$ by XRD in grazing incidence geometry, and the results are shown in Figure 7. Although, from the morphological point of view, the $200\text{ }^\circ\text{C}$ annealing does not significantly modify the nanosized structure of the blocking layer (see comments of Figure 5) and its porosity, on the other hand, the lattice structure and the layer composition are drastically modified. Increasing the annealing temperature to $500\text{ }^\circ\text{C}$ triggers further changes in the TiO_2 layer structure. In the diffraction pattern of Figure 7 some AZO peaks are present due to the fact that the blocking layer is thin, and at the angle used, the X-ray beam penetrates also into the AZO

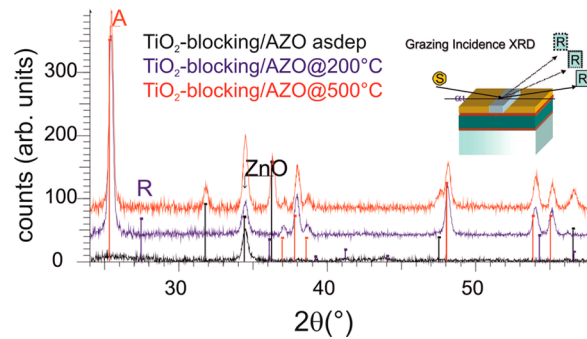


Figure 7. Grazing incidence XRD on the TiO_2 -blocking/AZO bilayer structure. The TiO_2 layer composition and the domain size change as a function of the pretreatments done on the TiO_2 -blocking/AZO bilayer before mesoscopic layer deposition.

layer. Not all the AZO peaks are present (see the reference marks of the powder) due to the AZO fiber texturing along the [0001] zone axis.¹⁵ From Figure 7 it is noteworthy that the composition of the layer changes as a result of the annealing process. Anatase and a very little amount of rutile are present in the as deposited layer, while, after annealing, anatase dominates as the only polymorphism in the layer.

In Figure 8a, the texture coefficient $J = (I_{hkl}/I_{hkl}^*)/(\sum_{hkl}(I_{hkl}/I_{hkl}^*))$, where I^* is the expected intensity in a reference powder as extracted from the data in Figure 7, is represented as a function of the Bragg angle (the different peaks of R and A). This parameter gives an indication of the eventual occurrence

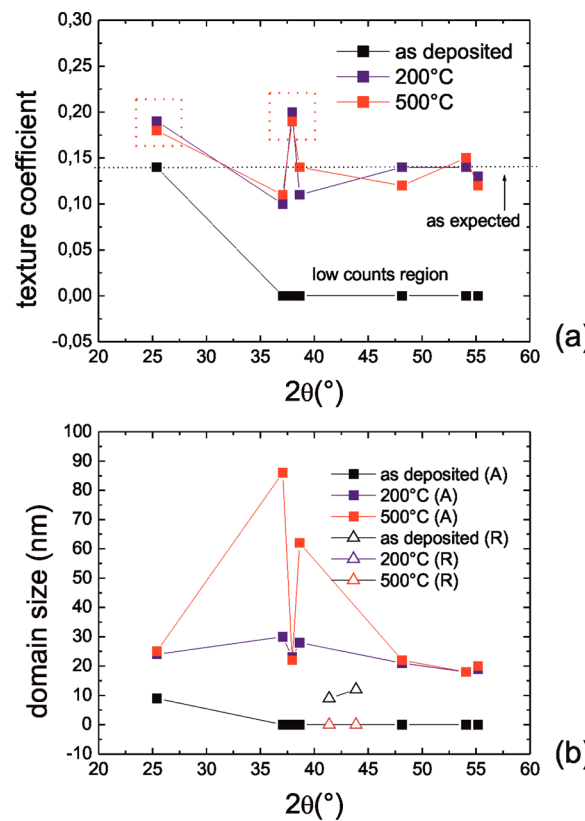


Figure 8. (a) Texture coefficient and (b) domains size for R and A at different Bragg angles of the TiO_2 -blocking layer deposited on the AZO substrate, as extracted from the grazing incidence diffraction patterns.

of preferential orientations in a polycrystalline structure, by taking into account the scattering factors for each hkl plane. From the analyses, it emerges that, in both the annealed blocking layers, the anatase domains are not randomly oriented (see values associated with the (101) and (400) planes). Anatase nucleation and growth triggered by preferentially oriented AZO substrates (e.g., [0001]) is a result expected on the basis of our previous data, at least for annealing up to 200 °C.¹⁵ Small differences in the texturing properties of this TiO₂ layer can be encountered by slightly modifying the surface exposed by the AZO to the TiO₂ deposition process (under investigation). The occurrence of a texturing implies that the TiO₂/AZO interface is not randomly arranged, especially after annealing, but it rather gains a certain degree of uniformity, which thus could reflect in a minor resistance to the carrier transport through it.

Increasing the annealing temperature from 200 to 500 °C does not alter the preferential texturing of the anatase domains. Although the texturing coefficient does not change significantly with the annealing temperature, on the other hand, the domains size is severely modified by the annealing, with a trend which depends on the temperature used to treat the TiO₂-blocking/AZO bilayer before mesoscopic layer deposition. The data in Figure 8b show, in fact, that after annealing at 200 °C the average domain size of the anatase polymorphism increases from ~10 to ~20 nm; after annealing at 500 °C the domain size can also get, for some particular grain orientation, an average diameter of 85 nm. Very large TiO₂ domains were, in fact, detected by TEM plan view analyses (see Figure 6b).

In Figure 9, the relative changes of the interplanar distances of the anatase planes in the TiO₂-blocking layer as a function of

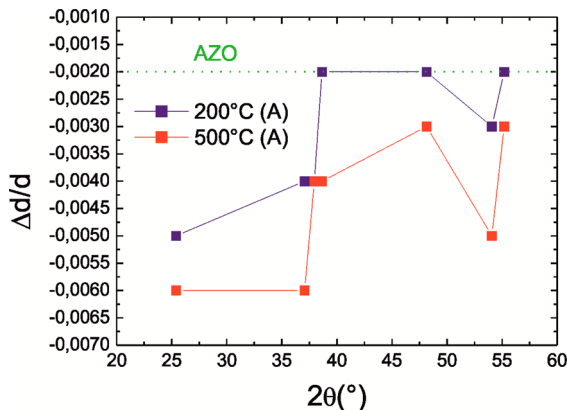


Figure 9. Relative changes of the interplanar distances of anatase planes in the TiO₂-blocking layer at different Bragg angles, as extracted by the grazing incidence diffraction pattern. The values were calculated from the peak position, using the Bragg relationship.

the Bragg angles are shown after 200 and 500 °C annealing, before mesoscopic layer deposition. A unique AZO reference is also indicated since the peak position is not affected by the annealing process. It can be observed that (1) the anatase domains are under compressive strain and (2) the average compressive strain increases after annealing at 500 °C, similarly to what observed for the grain size.

It can be thus summarized that: (1) rutile and anatase domains are already present in the TiO₂-blocking layer after deposition, although the deposition temperature (150 °C) is low (they are not expected at such a low T);^{31,32} (2) R get preferential orientations: note, in fact, that the contribution

from the (110) planes ($I = 100\%$) is quite low; (3) the size of the R and A domains in the as deposited TiO₂-blocking layer is small (~9 nm); (4) rutile is consumed during annealing by anatase: no residual R phase is observed after 200 °C annealing; (5) the size of the anatase domains increases with T ; (6) large TiO₂ domains are formed after 500 °C annealing: they are well structured without defects

3.5. X-ray Reflectivity and Optical Transmittance of the TiO₂-Blocking/AZO Bilayer. The TiO₂-blocking/AZO bilayer reflectivity behavior under X-ray irradiation is, as expected, affected by the electronic density of the blocking layer, and also can give some information on the AZO layer underneath. This is shown in Figure 10a, wherein the first drop,

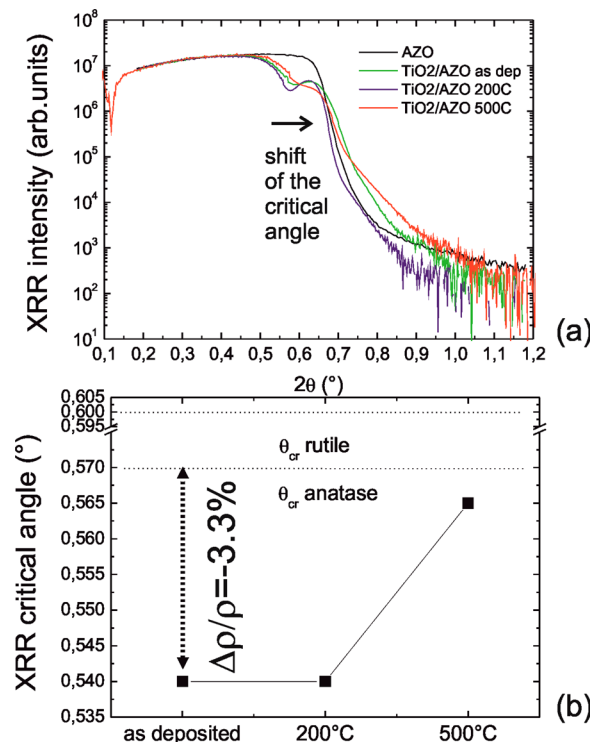


Figure 10. (a) X-ray reflectivity of the TiO₂-blocking/AZO bilayer as a function of the thermal treatment before mesoscopic layer deposition. The AZO reference, without any blocking layer above, is also shown. (b) Critical angle (θ_{cr}) in the different samples: the increase of the critical angle indicates a reduction of the layer porosity with a variation of the electronic density of the TiO₂ layer of 3.3%.

after the total reflection plateau, is due to the beam penetrating into TiO₂ layer while the second sudden drop is due to the X-ray beam starting to penetrate into the AZO substrate. The critical angle (taken at $I_{max}/2$, by definition) gives a measure of the material density. In this respect, the AZO critical angle does not suffer from the annealing process (see in comparison with the reference, without any blocking TiO₂ layer on top): the spreading of the signal is rather due to an increase of the surface roughness (which is also symmetrically registered around the TiO₂ critical angle). From the critical angle of the TiO₂ layer it can be argued that the density of that layer increases after postdeposition annealing at 500 °C. Since the layer stoichiometry and polymorphism do not change, it can be thus argued that the annealing improves the layer average compactness. This finding is in agreement with the increase of the average domain size in the TiO₂ layer registered by TEM

and XRD analyses. In Figure 10b, the relative changes of the average layer density are also shown, with the maximum variation registered at 500 °C (3.3%). It is also to note that the TiO₂ layer density after annealing closely approach that expected for the anatase phase, according to the layer composition.

The optical transmittance of the bilayer was also evaluated by UV-vis analyses, and the results are shown in Figure 11. The

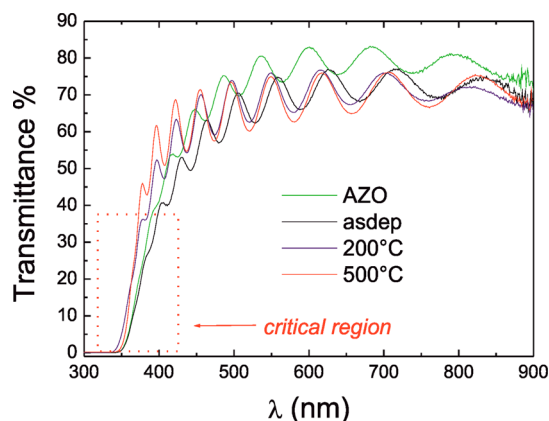


Figure 11. Optical transmittance of the TiO₂-blocking/AZO bilayer in the UV-vis range as a function of the thermal treatment before mesoscopic layer deposition. The AZO reference, without any blocking layer above, is also shown. The critical region indicates the range wherein the effects of the lattice defects recovery are visible.

reference AZO transmittance above 450 nm settles between 70 and 80% of the incident intensity. The TiO₂ layer deposited over the AZO substrate only slightly decreases the electrode transparency. Annealing the bilayer has the positive effect of improving the bilayer transmittance between 350 and 400 nm, and this was explained by a thermally induced process of defects recovery in the semiconductor layers.^{23,33} As a consequence of that, the $T(\lambda)$ curve becomes steeper above the absorption threshold (critical region indicated in the figure), and this occurs in both annealed bilayers (annealed at 200 and 500 °C). The evidence of the occurrence of a process of structural defects recovery, which thus causes a narrowing of the density of optically efficacious states near the gap, is in agreement with the occurrence of a severe structural modification induced by the thermal treatments as indicated by X-ray diffraction and X-ray reflectivity analyses (already discussed).

3.6. EIS Analyses. EIS analyses³⁴ were done to evaluate the effect on the cells component conductivity of the structural modifications induced in the TiO₂-blocking/AZO bilayer by the thermal treatments before TiO₂ mesoscopic layer deposition and dye loading. The mesoscopic layer thickness used was 5 μm. The electrochemical impedance spectroscopy (EIS) data were recorded by scanning frequency of charging voltage at the cell with a computer-controlled potentiostat (VSP, Princeton Applied Research) from 200 kHz to 0.1 Hz with 10 mV amplitude at open circuit condition under 1 sun irradiation. The plot from EIS measurements for cells made with different conditions of TiO₂ blocking layer is shown in Figure 12. These data were fitted by the equivalent circuit model shown in the inset of Figure 12. Table 2 shows the results of fitted data for elements of resistance and capacity.

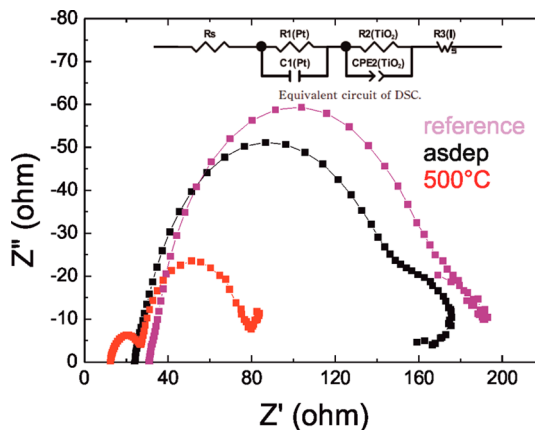


Figure 12. EIS analyses of the complete cells (mesoscopic layer thickness = 5 μm) as a function of the thermal treatment on the of the TiO₂-blocking/AZO bilayer before mesoscopic layer deposition. EIS measured were done at open circuit condition under 1 sun illumination.

Table 2. Fitting Results of EIS Data in Figure 12^a

cell no.	R _s (Ω)	R ₁ (Ω)	C ₁ (μF)	R ₂ (Ω)	CPE2-T (μF)	CPE2-P
(ref)	30.8	76.4	8.4	77.0	170	0.67
Asdep	24.1	21.3	890	128	14.4	0.83
500 °C	12.8	13.7	3.37	48.5	350	0.94

^aR_s: sum of internal resistance of the substrate and solution resistance; R₁: charge transfer resistance of counter electrode; C₁: capacitance of cathode; CPE2-T: constant of CPE of photoanode (TiO₂); CPE2-P: exponent of CPE of photoanode (TiO₂); R₂: charge transfer resistance of photoanode (TiO₂). R₁ is considered a constant, since the spread of the values are within the fitting errors. The R_s values are significantly reduced after annealing at 200 and 500 °C. R₂ gets the lowest value after 500 °C annealing due to a higher adhesion degree between the blocking layer and the mesoporous film.

Large semicircles in the plot are associated with the resistance R₂, which is due to carrier conduction at the interface of the blocking layer with the mesoporous TiO₂ and inside the mesoporous TiO₂ film. Intercept of the curves at Z'' = 0 indicates the series resistance (dc resistance), R_s, detected at high frequencies, which is normally due to resistances of the conductive substrates. It is first noted that the cell made with 500 °C treated TiO₂-blocking/AZO bilayer has the lowest values for R_s as well as for R₂. Those two values were thus respectively correlated to a reduction of the blocking/AZO bilayer resistance and to an improvement of the adhesion between the mesoporous array of TiO₂ nanograins and the compact layer, according to the structural findings (improved blocking layer compactness and increased TiO₂ grain size). Cells with blocking layers left as prepared or without the blocking layer exhibit progressively higher R_s values. This implies that, on one hand, the blocking layer has a beneficial effect on the collection of the carriers with respect to the case without any blocking and, on the other hand, that an annealing process before the mesoporous TiO₂ array deposition is suited to improve the electrode conductivity. This last finding was attributed to a general reduction of the blocking/AZO bilayer resistance after annealing. According to that, it was found, in fact, that the AZO sheet resistance changes from ~9 to ~6 ohm/sq after annealing at 500 °C (four-point probe). A trend is also encountered in the R₂ values, but since it derives from the fitting procedure of the double arc (R₁ and R₂), the more

accurate value is that extracted on the 500 °C annealed blocking/AZO bilayer.

4. CONCLUSIONS

We explored new strategies for low thermal budget/high efficiency dye-sensitized solar cells. AZO-based DSSC were fabricated by a mixed approach based on combining dehydration–condensation reaction of hydrogen-bonded TiO₂ particles and sputtering deposition methods. All the fabrication processes were taken under 200 °C.

It was found that the low temperature binder-free TiO₂ preparation method allows mesoporous TiO₂ formation on AZO substrates without damaging the TCO surface. This was a beneficial effect of the low temperature preparation method. Additionally, it was argued that a 40 nm thick and undoped TiO₂-blocking layer deposited by sputtering at $T < 200$ °C can have, once structurally optimized, a severe effect on the cell performances. The presented method allows overcoming the actual literature limit for AZO-based DSSC (3.8%) using a relatively thin (8 μm) mesoporous array of our low- T and undoped nano-TiO₂ grains. With this approach, the cell efficiency was even raised to 4.9%, as the blocking/AZO bilayer was pretreated at 500 °C 30 s, before mesoporous array deposition. It is, finally, noteworthy that this large efficiency can be roughly maintained (4.6%) by scaling the thermal budget for photoanode preparation from 500 to 200 °C, thus offering the opportunity of applying the multilayer materials on plastic substrates.

The cell performances were correlated to the TiO₂/AZO conductivity by means of the EIS analyses. Tuning in a proper way the structural properties of the blocking layer allows reducing the series contribution to the cell resistance and guaranteeing proper adhesion/protection to AZO against corrosion by the electrolytic solution, thus resulting in improved photovoltaic performances. In this respect, it was found that the compactness of the blocking layer, gained during annealing and accompanied by a grain size increase plus a texturing phenomenon of the anatase polymorphism, was useful to improve the electron collection efficiency of the cells and to reduce the parasitic diode contributions.

We intend to pass the message that AZO-based cells are currently not at the final state, but rather there is a quite large degree of possible adjustments by taking care about the materials science of the components and their coupling. Our low-temperature approach aims at the use of newly designed plastic substrates (e.g., HS-PEN)^{35,36} having tested process temperature even slightly above 200 °C.

■ AUTHOR INFORMATION

Corresponding Author

*Tel 0039 095 5968214, e-mail alessandra.alberti@imm.cnr.it (A.A.).

Notes

The authors declare no competing financial interest.

■ ACKNOWLEDGMENTS

The authors thank B. Cafra (STMicroelectronics) for the expert support in AZO depositions; M. Italia (CNR-IMM) for the RTA processes; F. Roccaforte, G. Greco, and S. Di Franco (CNR-IMM) for the fruitful discussions on the Ti/TiO₂ interface electrical contact; and Marco Torrisi (STMicroelectronics) for cross-sectional TEM samples preparation by

focused ion beam. This work was partially funded by MIUR by means of the national Program PON R&C 2007-2013, project “Tecnologie per l’ENERGia e l’Efficienza energETICA (ENERGETIC)” (PON02_00355_3391233).

■ REFERENCES

- O'Reagan, B.; Graetzel, M. A Low-Cost, High-Efficiency Solar Cell Based on Dye-Sensitized Colloidal TiO₂ Films. *Nature* **1991**, *353*, 737–740.
- Tian, H.; Yu, X.; Zhang, J.; Duan, W.; Tian, F.; Yu, T. The Influence of Environmental Factors on DSSCs for BIPV. *Int. J. Electrochem. Sci.* **2012**, *7*, 4686–4691.
- Yella, A.; Lee, H.-W.; Tsao, H. N.; Yi, C.; Chandiran, A. K.; Nazeeruddin, M. K.; Diau, E. W.-G.; Yeh, C.-Y.; Zakeeruddin, S. M.; Grätzel, M. Porphyrin-Sensitized Solar Cells with Cobalt (II/III)-Based Redox Electrolyte Exceed 12% Efficiency. *Science* **2011**, *334*, 629–634.
- Liu, H.; Avrutin, V.; Izyumskaya, N.; Özgür, Ü.; Morkoç, H. Transparent Conducting Oxides for Electrode Applications in Light Emitting and Absorbing Devices. *Superlattices Microstruct.* **2010**, *48*, 458–484.
- Kijitora, Y.; Ikegami, M.; Miyasaka, T. Highly Efficient Plastic Dye-Sensitized Photoelectrodes Prepared by Low-Temperature Binder-Free Coating of Mesoscopic Titania Nano-Pastes. *Chem. Lett.* **2007**, *36*, 190–191.
- Miyasaka, T.; Ikegami, M.; Kijitora, Y. Photovoltaic Performance of Plastic Dye-Densitized Electrodes Prepared by Low-Temperature Binder-Free Coating of Mesoscopic Titania. *J. Electrochem. Soc.* **2007**, *154*, A455–461.
- Miyasaka, T.; Kijitora, Y.; Ikegami, M. Plastic Dye-Sensitized Photovoltaic Cells and Modules Based on Low-Temperature Preparation of Mesoscopic Titania Electrodes. *Electrochemistry* **2007**, *75*, 2–12.
- Miyasaka, T. Toward Printable Sensitized Mesoscopic Solar Cells: Light-Harvesting Management with Thin TiO₂ Films. *J. Phys. Chem. Lett.* **2011**, *2*, 262–269.
- Yu, H.; Zhang, S.; Zhao, H.; Xue, B.; Liu, P.; Will, G. High Performance TiO₂ Photoanode with an Efficient Electron Transport Network for Dye-Sensitized Solar Cells. *J. Phys. Chem. C* **2009**, *113*, 16277–16282.
- Wua, M.-S.; Tsaia, C.-H.; Jowa, J.-J.; Weib, T.-C. Enhanced Performance of Dye-Sensitized Solar Cell via Surface Modification of Mesoporous TiO₂ Photoanode with Electrodeposited Thin TiO₂ Layer. *Electrochim. Acta* **2011**, *56*, 8906–8911.
- Wu, M.-S.; Tsai, C.-H.; Wei, T.-C. Electrochemical Formation of Transparent Nanostructured TiO₂ Film as an Effective Bifunctional Layer for Dye-Sensitized Solar Cells. *Chem. Commun.* **2011**, *47*, 2871–2873.
- Miyoshi, K.; Numao, M.; Ikegami, M.; Miyasaka, T. Effect of Thin TiO₂ Buffer Layer on the Performance of Plastic-Based Dye-Sensitized Solar Cells Using Indoline Dye. *Electrochemistry* **2008**, *76*, 158.
- Kavan, L.; Tetrelaut, N.; Moehl, T.; Gratzel, M. Electrochemical Characterization of TiO₂ Blocking Layers for Dye-Sensitized Solar Cells. *J. Phys. Chem. C* **2014**, DOI: 10.1021/jp4103614.
- Pellegrino, G.; Condorelli, G.-G.; Privitera, V.; Cafra, B.; Di Marco, S.; Alberti, A. Dye-Sensitizing of Self-Nanostructured Ti(·Zn)-O₂/AZO Transparent Electrodes by Self-Assembly of 5,10,15,20-Tetrakis(4-carboxyphenyl)porphyrin (TCPP). *J. Phys. Chem. C* **2011**, *115*, 7760–7767.
- Pellegrino, G.; Bongiorno, C.; Ravesi, S.; Alberti, A. Fiber Texturing in Nano-Crystalline TiO₂ Thin Films Deposited at 150 °C by DC Reactive Sputtering on Fiber-Textured [0001] ZnO:Al Substrates. *J. Phys. D: Appl. Phys.* **2012**, *45*, 355301–6.
- Pellegrino, G.; Alberti, A.; Condorelli, G. G.; Giannazzo, F.; La Magna, A.; Paoletti, A. M.; Pennesi, G.; Rossi, G.; Zanotti, G. Study of the Anchoring Process of Tethered Unsymmetrical Zn-Phthalocya-

- nines on TiO₂ Nanostructured Thin Films. *J. Phys. Chem. C* **2013**, *117*, 11176–11185.
- (17) Alberti, A.; Bongiorno, C.; Pellegrino, G. Anatase/Rutile Nucleation and Growth on (0002) and (11–20) Oriented ZnO:Al/Glass Substrates at 150 °C. *Thin Solid Films* **2014**, *555*, 3–8.
- (18) Pellegrino, G.; Condorelli, G. G.; De Rossi, F.; Brown, T.; Giovenale, F.; Bongiorno, C.; Alberti, A. Thermally Induced Structural Modifications of Nano-Sized Anatase Films and the Effects on the Dye-TiO₂ Surface Interactions. *Appl. Surf. Sci.* **2014**, DOI: 10.1016/j.apsusc.2014.01.042.
- (19) Mohamed, S. H.; Kappertz, O.; Leervard Perdersen, T. P.; Drese, R.; Wuttig, M. Properties of TiO_x Coatings Prepared by DC Magnetron Sputtering. *Phys. Status Solidi A* **2013**, *198*, 224–237.
- (20) Gago, R.; Redondo-Cubero, A.; Vinnichenko, M.; Vazquez, L. Annealing of Heterogeneous Phase TiO₂ Films: An X-Ray Absorption and Morphological Study. *Chem. Phys. Lett.* **2011**, *511*, 367–371.
- (21) Gago, R.; Vinnichenko, M.; Redondo-Cubero, A.; Czgany, Z.; Vazquez, L. Surface Morphology of Heterogeneous Nanocrystalline Rutile/Amorphous Anatase TiO₂ Films Grown by Reactive Pulsed Magnetron Sputtering. *Plasma Processes Polym.* **2010**, *7*, 813–823.
- (22) Musil, J.; Herman, D.; Sicha, J. Low-Temperature Sputtering of Crystalline TiO₂ Films. *J. Vac. Sci. Technol., A* **2006**, *24*, 521–528.
- (23) Landmann, M.; Köhler, T.; Köppen, S.; Rauls, E.; Frauenheim, T.; Schmidt, W. G. Fingerprints of Order and Disorder in the Electronic and Optical Properties of Crystalline and Amorphous TiO₂. *Phys. Rev. B* **2012**, *86*, 064201:1–20.
- (24) Noh, J.-H.; Han, H. S.; Lee, S.; Kim, D. H.; Park, J. H.; Park, S.; Kim, J. Y.; Jung, H. S.; Hong, K. S. A Newly Designed Nb-Doped TiO₂/Al-Doped ZnO Transparent Conducting Oxide Multilayer for Electrochemical Photoenergy Conversion Devices. *J. Phys. Chem. C* **2010**, *114*, 13867–13871.
- (25) Qi, J.-H.; Li, Y.; Duong, T.-T.; Choi, H.-J.; Yoon, S.-G. Dye-Sensitized Solar Cell Based on AZO/Ag/AZO Multilayer Transparent Conductive Oxide Film. *J. Alloys Compd.* **2013**, *556*, 121–126.
- (26) Zhang, D.; Yoshida, T.; Oekermann, T.; Furuta, K.; Minoura, H. Room-Temperature Synthesis of Porous Nanoparticulate TiO₂ Films for Flexible Dye-Sensitized Solar Cells. *Adv. Funct. Mater.* **2006**, *16*, 1228–1234.
- (27) Park, N.-G.; Kim, K. M.; Kang, M. G.; Ryu, K. S.; Chang, S. H.; Shin, Y.-J. Chemical Sintering of Nanoparticles: A Methodology for Low-Temperature Fabrication of Dye-Sensitized TiO₂ Films. *Adv. Mater.* **2005**, *17*, 2349–2353.
- (28) Zardetto, V.; Di Giacomo, F.; Garcia-Alonso, D.; Keuning, W.; Creatore, M.; Mazzuca, C.; Reale, A.; Di Carlo, A.; M. Brown, T. Fully Plastic Dye Solar Cell Devices by Low Temperature UV-Irradiation of Both the Mesoporous TiO₂ Photo- and Platinized Counter-Electrodes. *Adv. Energy Mater.* **2013**, *3*, 1292–1298.
- (29) Spurr, R. A.; Myers, H. Quantitative Analysis of Anatase-Rutile Mixtures with an X-Ray Diffractometer. *Anal. Chem.* **1957**, *29*, 760–762.
- (30) Hanaor, D. A. H.; Sorrell, C. C. Review of the Anatase to Rutile Phase Transformation. *Mater. Sci.* **2011**, *46*, 855–874.
- (31) Senthilkumar, V.; Jayachandran, M.; Sanieeviraja, C. Preparation of Anatase TiO₂ Thin Films for Dye-Sensitized Solar Cells by DC Reactive Magnetron Sputtering Technique. *Thin Solid Films* **2010**, *519*, 991–994.
- (32) Zhang, Y.; Ma, X.; Chen, P.; Yang, D. Effect of the Substrate Temperature on the Crystallization of TiO₂ Films Prepared by DC Reactive Magnetron Sputtering. *J. Cryst. Growth* **2007**, *300*, 551–554.
- (33) Mo, S.-D.; Ching, W. Y. Electronic and Optical Properties of Three Phases of Titanium Dioxide: Rutile, Anatase, and Brookite. *Phys. Rev. B* **1995**, *51*, 13023–13032.
- (34) Wu, M.-S.; Tsai, C.-H.; Wie, T.-C. Electrochemical Formation of Transparent Nanostructured TiO₂ Film as an Effective Bifunctional Layer for Dye-Sensitized Solar Cells. *Chem. Commun.* **2011**, *47*, 2871–2873.
- (35) MacDonald, W. A.; Looney, M. K.; MacKerron, D.; Eveson, R.; Adam, R.; Hashimoto, K.; Rakos, K. Latest Advances in Substrates for Flexible Electronics. *J. SID* **2007**, *15/12*, 1075–1083.
- (36) Zardetto, V.; Brown, T. M.; Reale, A.; Di Carlo, A. Substrates for Flexible Electronics: A Practical Investigation on the Electrical, Film Flexibility, Optical, Temperature, and Solvent Resistance Properties. *J. Polym. Sci., Polym. Phys.* **2011**, *49*, 638–648.